VII International Conference on Computational Methods in Marine Engineering
MARINE 2017
M. Visonneau, P. Queuteyand and D. Le Touzé (Eds)

EFFECTS OF BLADE GEOMETRY ON CAVITATION AND PRESSURE FLUCTUATIONS OF TUNNEL THRUSTERS

CHENG YU, XIAO-QIAN DONG*, WEI LI, CHEN-JUN YANG

State Key Laboratory of Ocean Engineering(SKLOE)
Collaborative Innovation Center for Advanced Ship and Deep-Sea Exploration(CISSE)
Shanghai Jiao Tong University, Shanghai 200240, China
*Email: xiaoqiandong0330@sjtu.edu.cn

Key words: tunnel thruster, model test, CFD, blade geometry, cavitation, fluctuating pressure

ABSTRACT: Compared with open propellers, tunnel thruster blades are more vulnerable to cavitation and local structure vibration problems because they are typically heavily loaded and subject to severe non-uniformity of inflow produced by the blunt gearbox. However, it seems that the simple 'flat plate' is still often used in designing the thruster blades. In this research, model tests and RANS simulations are carried out for three highly skewed thruster blades having different pitch and rake profiles to investigate the effects of blade geometry on cavitation and pressure fluctuations. The results indicate that the 'flat plate' blade is unfavorable for vibration excitation and unloading towards the tip is an effective way to reduce the fluctuating pressures.

1 INTRODUCTION

Ship vibration can bring about structural damage, fatigue, excessive noise and other issues. The major sources of excitation include the propeller, main engine, and waves, where the propeller is usually the most important one. Once cavitation happens, the propeller induced fluctuating pressures will increase significantly and such problems are among the most active research topics in ship propulsion.

For open propellers, relevant researches based on both model experiments and numerical simulations are relatively sufficient. For example, Pereira *et al*.[1,2] conducted fluctuating pressure and noise measurements for a cavitating propeller in uniform and non-uniform flows and demonstrated that the pressure fluctuations due to the occurrence of cavitation are proportional to the cavity volume acceleration by the test results. Salvatore *et al*.[3] compared seven computational models including RANS, LES, and BEM for the INSEAN E779A propeller in uniform and non-uniform inflows. The comparison of numerical results highlights a good agreement for the non-cavitating steady flow predictions, whereas for the cavitating flow, discrepancies in cavity extent are observed. The main reason is likely to be the lack of grid density and/or too much numerical dissipation in the vicinity of the cavity-fluid interface.

However, the relevant researches on tunnel thrusters seem to be scarcely available in the public domain due to high loading on the impeller blades and interactions among different parts of the thruster. The typical configuration of a tunnel thruster includes an impeller, a T-shaped

housing (the 'gearbox' hereinafter) of the right-angle shaft system, and a driving motor. Due to the limited space available, the gearbox is typically blunt in geometry and close to the impeller blades, which induces severe blockage effect and flow non-uniformity for the impeller. Meanwhile, the impeller blades are usually heavily loaded. Under such adverse conditions tunnel thrusters are more vulnerable to cavitation, especially when the simple 'flat plate' impeller blades are used. The fluctuating pressures induced by the impeller on the tunnel wall can exceed those by a propeller on the stern by two orders of magnitude when cavitation happens.

There are just a few pieces of work, all published in the 1960s, focusing on the hydrodynamic performance of tunnel thrusters based on model experiments[4] and design methods[5~7]. During the last ten years advances in computational fluid dynamics have made it possible to simulate the viscous flow of tunnel thrusters[8~10]. Unfortunately, the research work on cavitation and its induced effects is still scarce in the public domain. Stefano *et al*.[11] investigated the hydrodynamic performance and cavity patterns for a 'flat plate' Kaplan type propeller working in a cylinder at two pitch settings, based on BEM simulation and experimental observation. Fischer[12] proposed a design criterion for tunnel thrusters from the perspective of reducing the vibration and noise and measured the noise levels in cabins. It has been found that noise and vibration levels are different depending on thrust direction and the noise is 5~10 dB higher in low frequency range when the gearbox is located upstream of the impeller.

As dynamic positioning systems are equipped on more ships and operate more frequently, the necessity becomes obvious to enhance the performance of thrusters. In this research, model tests and RANS simulations are carried out for three highly skewed thruster blades having different pitch and rake profiles to investigate the effects of blade geometry on cavitation and pressure fluctuations. The impeller models are designed to produce the same amount of thrust when fitted to the same gearbox and bow model. The fluctuating pressures on the tunnel wall are measured at a number of locations in the vicinity of the blade tip. Viscous flow CFD simulations are carried out for the three impellers in one condition to gain more detailed information of the flow.

2 EXPERIMENTAL RESEARCH

2.1 Test facility and measuring equipments

The model tests are carried out in the cavitation tunnel of Shanghai Jiao Tong University, as shown in Figure 1. The test section is 6.1m in length, and its cross section is 1m×1m with rounded corners. The axial flow velocity over the test section ranges from 0.5m/s to 15.8m/s, and the static pressure at the centerline of the test section ranges from 25kPa to 300kPa. The non-uniformity of axial flow velocity is less than 1%.

As shown in Figure 2, the generic bow model is 0.58m long, with identical cross section geometry over the length and a tunnel in transverse direction to house the thruster. The bow model is made of plexiglass to facilitate observation of the flow and cavitation inside the tunnel. As illustrated in Figure 3, the bow model is installed at the streamwise center of the third

observation window, and at a height to ensure the impeller shaft axis is 0.5m above the bottom floor of the test section.

Figure 1: The cavitation tunnel of Shanghai Jiao Tong University

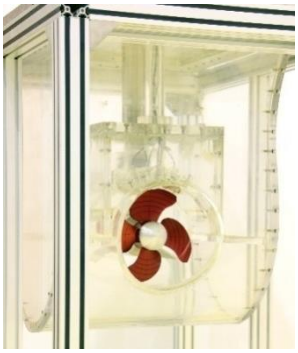

Figure 2: The generic bow model

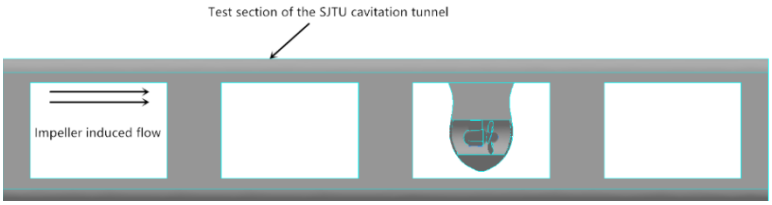

Figure 3: Setup of the bow model

As illustrated in Figure 4, six pressure transducers are installed on the tunnel wall, with the measuring surfaces flush with the inner wall surface. They are numbered as S1 through S6. Transducers S2 through S5 are located in the plane perpendicular to the shaft axis, and passing the mid-chord point of the tip section. Circumferentially, the four transducers are arranged symmetrically port and starboard at a spacing of 12°. Transducers S1 and S6 are arranged at 12 o'clock position, 0.127*D* upstream and downstream of the plane where S2 through S5 are arranged. Here *D* denotes the impeller diameter.

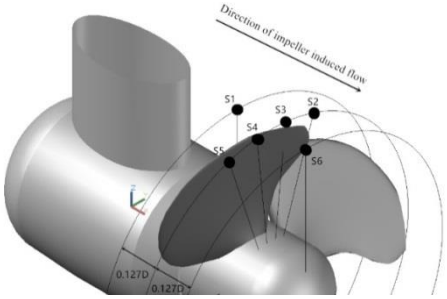

Figure 4: Arrangement of pressure transducers

The fluctuating pressures are measured with CYG505AFM micro pressure transducers made by Kunshan-ShuangQiao, a company in China. The measurable pressure range is 0~800kPa, and the accuracy and hysteresis repeatability are 0.5% and 0.05%, respectively. For the acquisition and analysis of the pressure signals, the PXIe-4331 multi-channel synchronous signal acquisition instrument made by National Instrument is utilized. The gain error is 0.1% of the reading and the offset error is 198μV/Vex. Figure 5 shows the equipments for pressure measurements.

Figure 5: Equipments for fluctuating pressure measurement

2.2 Impeller models

Three impeller models, named P1, P2, and P3 respectively, are utilized for the present research to investigate the effects of pitch distribution and local rake near the tip of blade. They were designed to produce the same amount of thrust at the same speed of rotation. According to our RANS simulations, the thrust coefficients of impellers P1, P2, and P3 are 0.183, 0.182, and 0.183, respectively.

Table 1: Main particulars of impeller models

Impellermodel	P1	P2	P3
Direction of rotation	Left-handed		
Number of blades	4		
Diameter(mm)	250		
Hub ratio	0.4		
Expanded area ratio	0.6		
Pitch ratio at 0.7*R*	0.75	0.89	0.89
Tip skew angle (deg.)	22.8		
Tip rake(mm)	0	-7.3	-7.3
Blade section	Symmetrical		
Tip clearance (mm)	1.6		

The main particulars of the three impellers are listed in Table 1, where *R* is the impeller tip radius, *R*=*D*/2. Impeller P1 is the traditional 'flat plate' design, *i.e.*, the blade mean

surface is a flat one (rather than a helical surface). The blades of P1 are rotated around their respective generator lines by 18.83° (from zero pitch). Impellers P2 and P3 were designed like a fixed pitch propeller with unloaded tips to improve cavitation performance. As shown in Figure 6, P2 and P3 share the same pitch distribution, which is quite different from that of P1. The three impellers share the same skew distribution, as shown in Figure 7. Impeller P2 differs from P3 only in total rake distribution, as shown in Figure 8. The former has a linear rake, while the latter has a sudden change in rake at 0.9*R* so that the tip region is bent towards upstream to alleviate the tip leakage vortex flow. Figure 9 shows the test models which are made from aluminum alloy with the surfaces anodized.

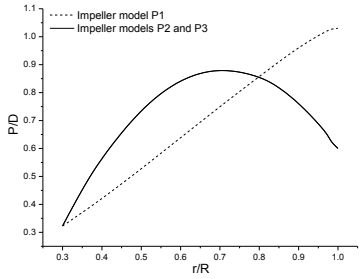

Figure 6: Comparison of pitch distributions

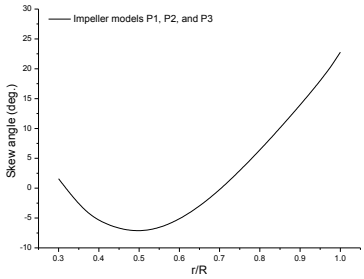

Figure 7: Skew distribution of impeller models

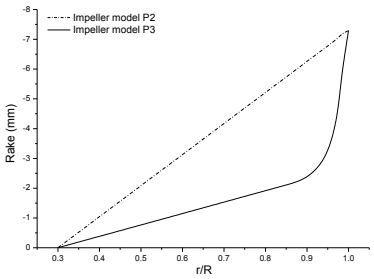

Figure 8: Rake distributions of impeller P2 and P3

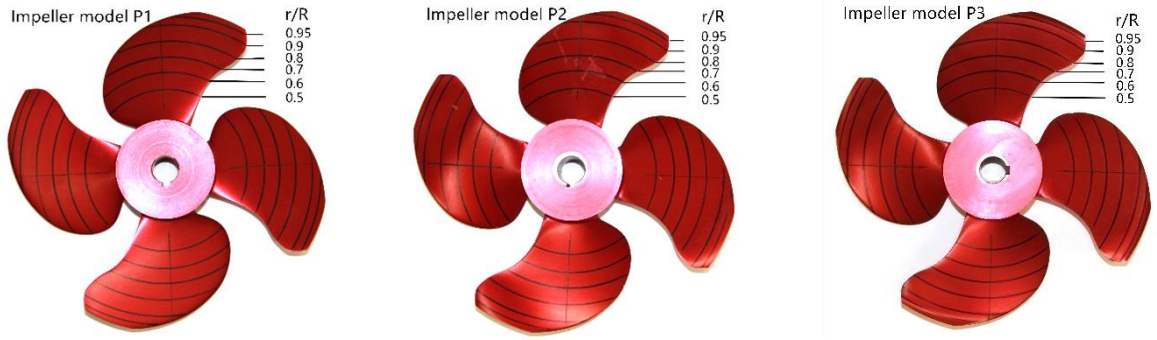

Figure 9: The impeller models for fluctuating pressure tests

2.3 Test results and analysis

2.3.1 Pre-test on the influences of flow speed and impeller rotation speed

The influences of flow speed and impeller rotation speed are investigated using impeller model P1. Tests are carried out at non-cavitating condition, where the absolute pressure of test section is 175kPa. The test conditions are listed in Table 2. For condition A and B, the impeller model works in 'quasi-bollard' condition, *i.e.*, the test section inlet flow velocity, *V*, is induced only by the tunnel thruster model. In condition C, the impeller of the cavitation tunnel rotates at a low speed, the inlet velocity is induced by both the tunnel thruster model and the impeller

of the cavitation tunnel.

Table 2: Test conditions for investigating influences of impeller and inflow speeds

Test condition	P_0 (kPa)	n (r/s)	V (m/s)
A	175	18	0.438
B	175	22.5	0.546
C	175	18	1.022

The fluctuating pressure coefficient is defined as

$$C_p = \frac{p - \bar{p}}{\frac{1}{2}\rho n^2 D^2} \tag{1}$$

where p is the measured absolute pressure, and $\bar{p}$ is the time average of p.

In Figure 10, a comparison is made for the total amplitude of fluctuating pressures coefficient, $\tilde{C}_{pt}$, which is defined as

$$\tilde{C}_{pt} = \sqrt{\sum_{i=1}^{5} i\tilde{C}_{pi}^2} \tag{2}$$

where $\tilde{C}_{pi}$ denotes the i^{th} blade frequency harmonic component of fluctuating pressure coefficient obtained from Fourier analysis. The results in Figure 10 indicate that, within the range of test conditions shown in Table 2, the influences of flow speed and propeller rotation speed are almost negligible.

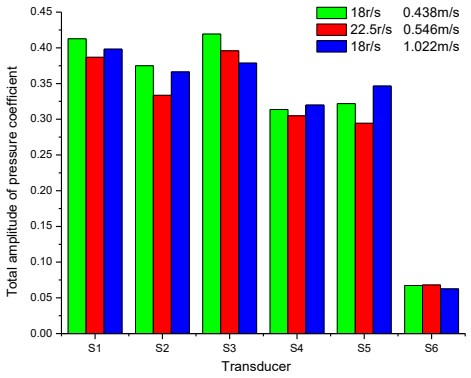

Figure 10: The influence of flow speed and propeller rotation speed on the total magnitude of fluctuating pressures for impeller model P1

2.3.2 Effects of blade geometry on pressure fluctuations

The tests on blade geometry effects are carried out in the 'quasi-bollard' condition. The rate of revolution, n, is set to be 22.5r/s based on considerations of the Reynolds number and the processing of fluctuating pressure data. At this rotating speed, the test section inlet flow velocities induced by the impeller model are 0.55m/s, 0.51m/s, and 0.51m/s for P1, P2, and P3 respectively. Based on the induced flow and impeller rotation speeds, the Reynolds numbers at $0.7R$ are equal to 3.6×10^6 for the three impellers. For each impeller, the fluctuating pressures

are measured at three conditions, σ_n=10.86, 3.75, and 2.5. The cavitation number, σ_n, is defined as

$$\sigma_n = \frac{p_0 - p_v}{\frac{1}{2}\rho n^2 D^2} \tag{1}$$

where p_0 is the static pressure at the shaft axis, p_v is the vapor pressure of water, and ρ is the density of water.

- **Cavity patterns**

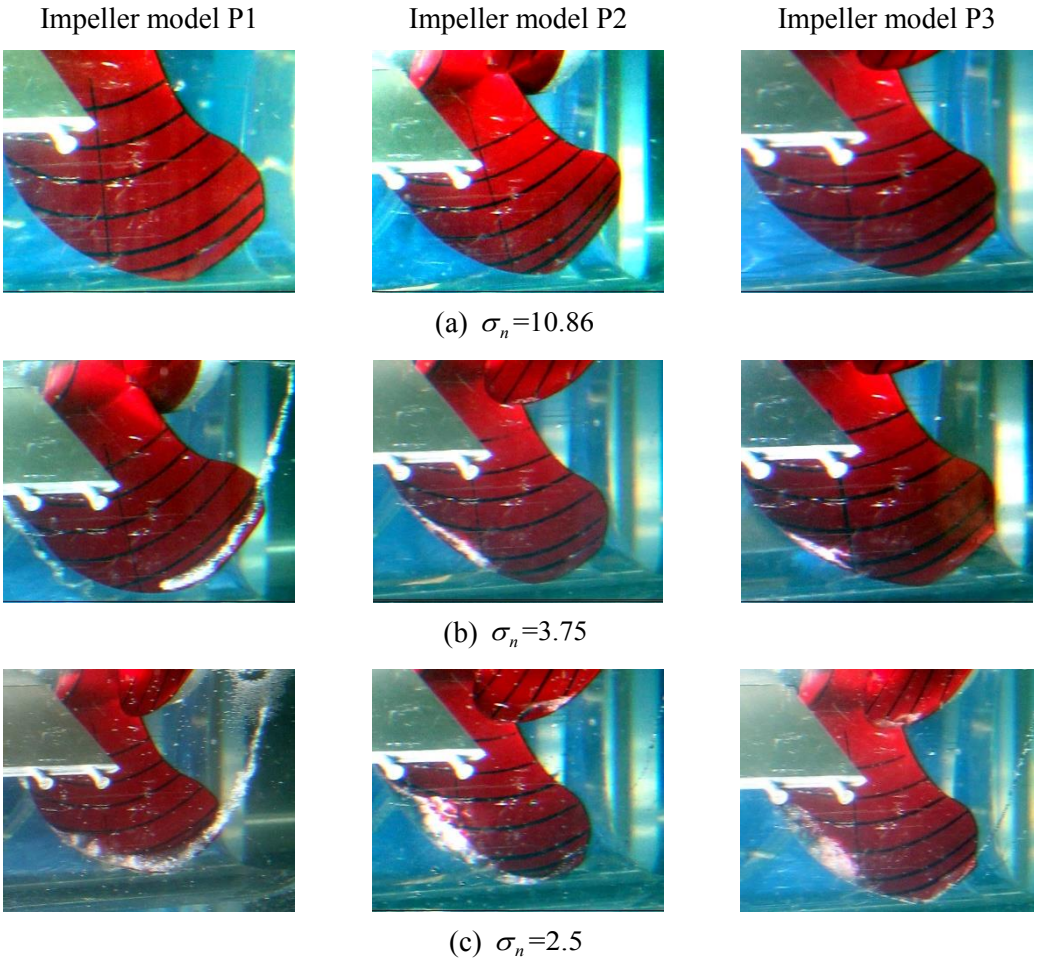

Figure 11: Comparison of cavity patterns in different cavitation conditions

Figure 11 shows the cavity patterns on the three impellers in different cavitation conditions. No cavity is observed at σ_n=10.86. At σ_n=3.75, the tip vortex cavity is already quite strong on impeller model P1, however, no tip vortex cavity is observed on impeller models P2 and P3, but some sheet cavity is observed instead. As the cavitation number decreases further to 2.5, for impeller P1, cavitation begins earlier in both radial and chordwise directions and develops into a sheet cavity, and the tip vortex cavity also becomes stronger. At the same cavitation

number, σ_n=2.5, the sheet cavity also becomes more extensive on impeller models P2 and P3, however the tip vortex cavities are still not obvious. The cavity patterns indicate that reducing the loading and using the nonlinear rake towards the tip, which is the case with P2 and P3 (see Figure 6 and Figure 8), can suppress the tip vortex cavitation, although the sheet cavitation in mid-radius region can become more extensive due to higher loading in that region.

- **Fluctuating pressures**

Figure 12 shows the fluctuating pressure amplitudes at transducer S1, where the 1st blade frequency harmonic dominates. In non-cavitating condition, impeller P3 is clearly superior to P2 and P1 in terms of the pressure amplitude; however, when cavitation exists, both P2 and P3 are better than P1, and P2 is the best. At transducer S6, the downstream one, the pressure amplitudes of P3 are mostly the lowest compared with P2 and P1, as shown in Figure 13.

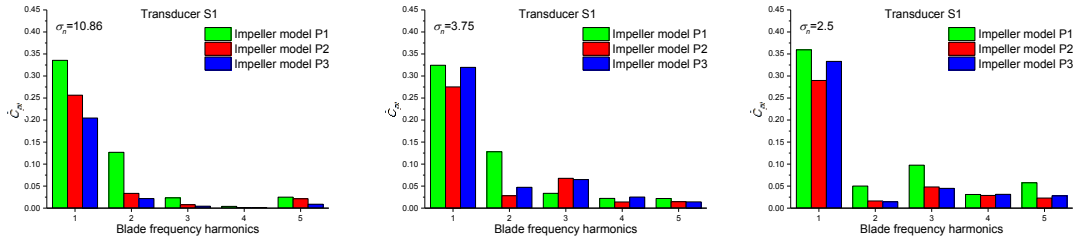

Figure 12: Comparison of fluctuating pressure amplitudes at transducer S1 in non-cavitating and cavitating conditions

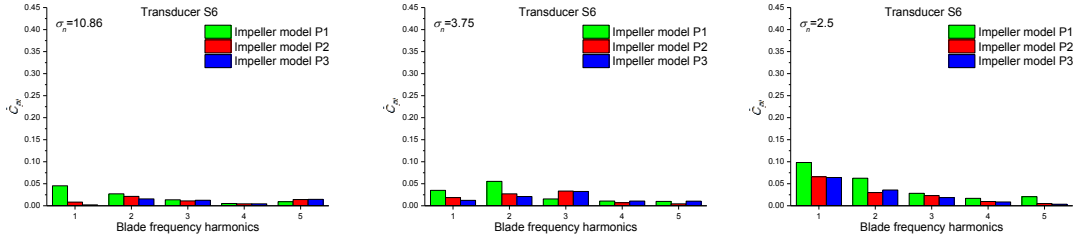

Figure 13: Comparison of fluctuating pressure amplitudes at transducer S6 in non-cavitating and cavitating conditions

Figure 14 through Figure 16 compare the fluctuating pressure amplitudes of the three impellers at transducers S2 through S5 in non-cavitating and cavitating conditions. For impeller P1, the fluctuating pressure amplitudes increase significantly as the cavitation number decreases. However, this tendency is not obvious for P2 and P3. In general, the pressure amplitudes of P1 are higher than those of P2 and P3, especially at the 1st and 2nd blade frequency harmonics.

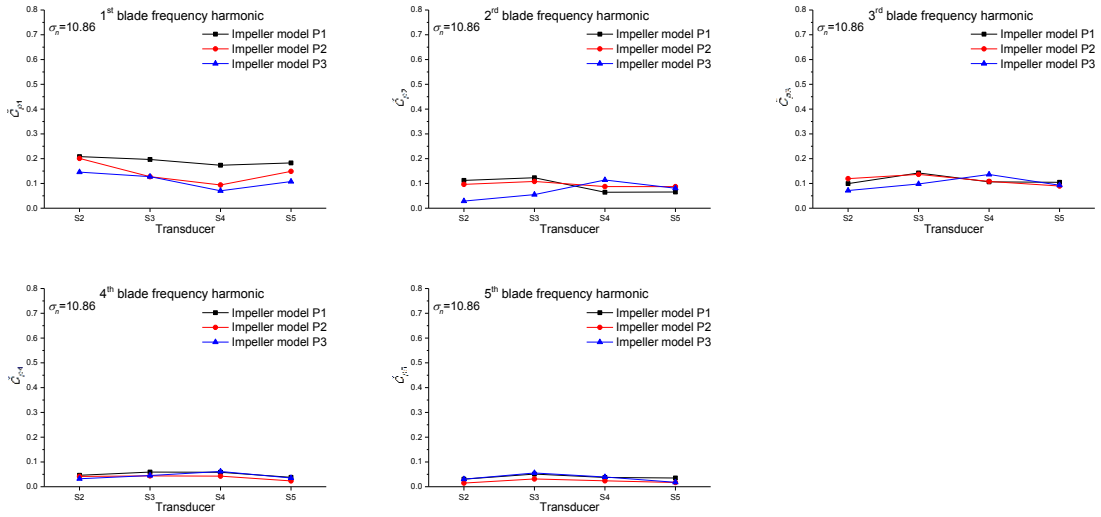

Figure 14: Comparison of fluctuating pressure amplitudes at transducers S2 through S5 in non-cavitating condition, σ_n =10.86.

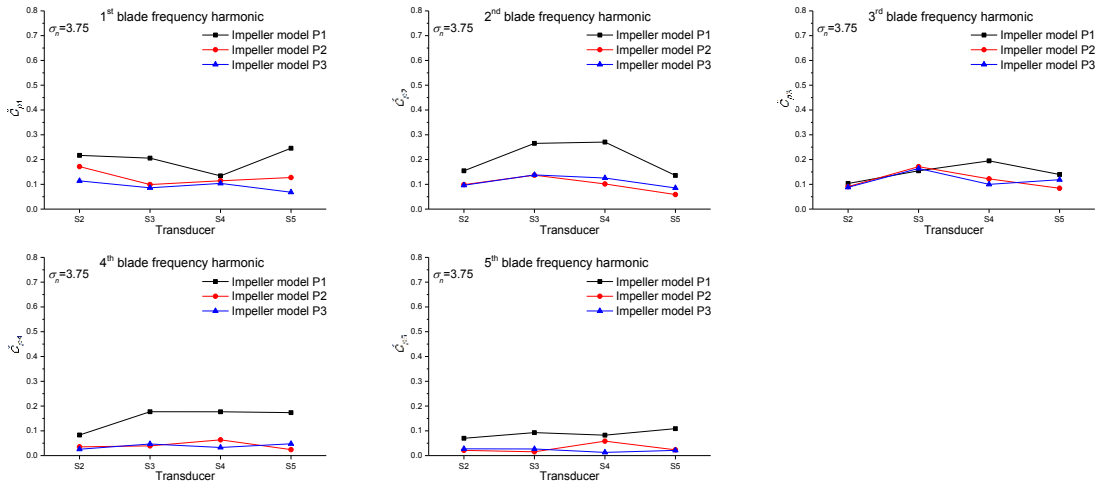

Figure 15: Comparison of fluctuating pressure amplitudes at transducers S2 through S5 in cavitating condition, σ_n =3.75.

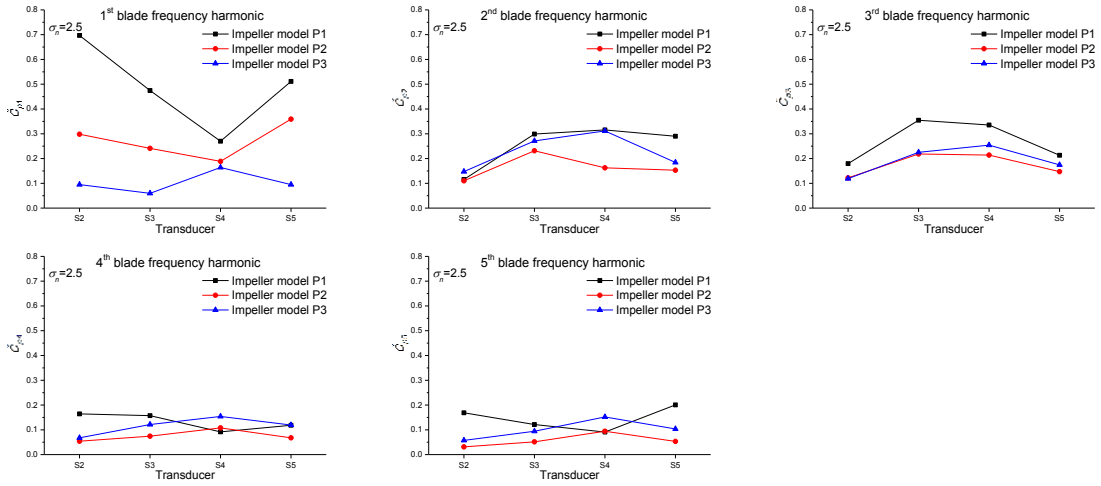

Figure 16: Comparison of fluctuating pressure amplitudes at transducers S2 through S5 in cavitating condition, σ_n =2.5

Figure 17 shows the comparison of the total amplitude of fluctuating pressures at the six transducer locations. The result is clear that the fluctuating pressure amplitudes of impeller P1 are higher than those of P2 and P3 in both cavitating and non-cavitating conditions and at all the measuring locations, which suggests that unloading the impeller blade towards the tip is an effective way to reduce the fluctuating pressures on the tunnel wall. In terms of the total amplitudes P2 and P3 are very close to each other, with only one exception at transducer S4, σ_n=2.5. In Figure 16, the fluctuating pressure amplitudes on transducer S4 are quite different from those on other transducers at the 1st and 2nd blade frequency harmonics, but the reason is not clear. Further study is necessary to find out if the rake distribution close to the tip can be further improved.

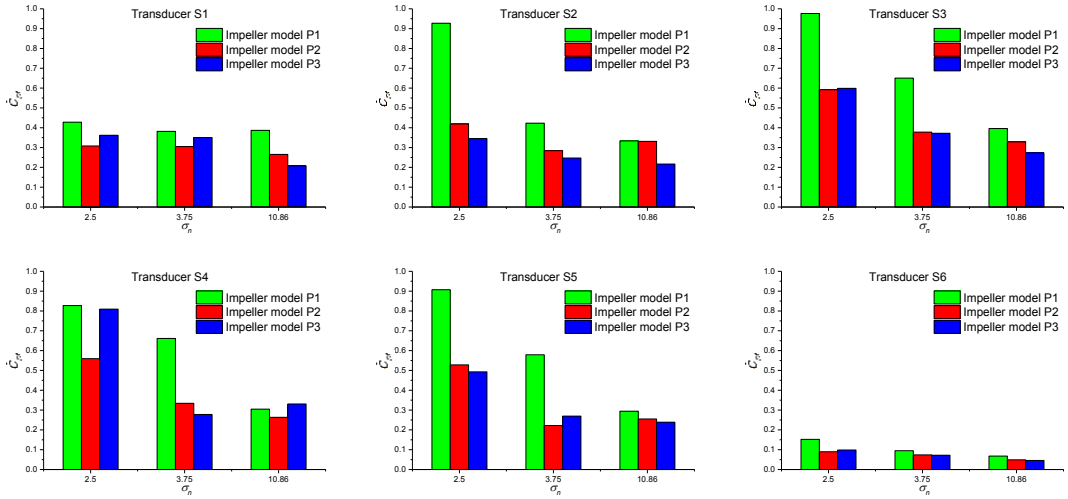

Figure 17: Comparison of the total amplitudes of fluctuating pressures

3 NUMERICAL SIMULATION

3.1 Modeling approach

Numerical simulations are conducted for the three impellers at σ_n=2.5, at rotating speed n=22.5r/s by using the commercial CFD software FLUENT.

The geometric model of the tunnel thruster is illustrated in the left part of Figure 18 together with the bow model for the present numerical computations. The hull is defined in a fixed rectangular coordinate system, O-XYZ, where the X axis points toward downstream, the Y axis points vertically upwards, and the Z axis completes the right-handed system. The origin, O, is located at the center of the impeller. The impeller rotates about the X axis in its positive direction by the right-hand rule. The computational domain is a cuboid with the size of 120D ×80D×40D, as illustrated in the right part of Figure 18. Such large domain is necessary to ensure the computational stability.

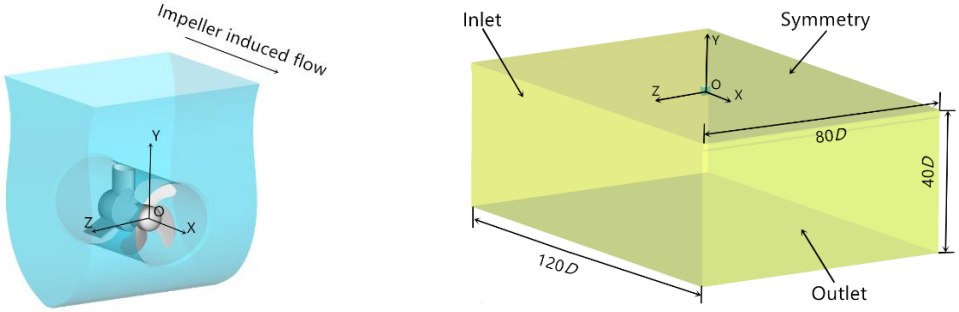

Figure 18: The geometric model of tunnel thruster (left) and the computational domain (right)

The computational domain is divided into two parts. The first part contains the impeller blades and the hub, which is defined in a coordinate system rotating synchronously with the impeller. As shown in Figure 19, the rotating part is discretized with tetrahedral cells. The average value of y^+ on blade surfaces is about 100, and the maximum skewness coefficient of the cells is 0.79.

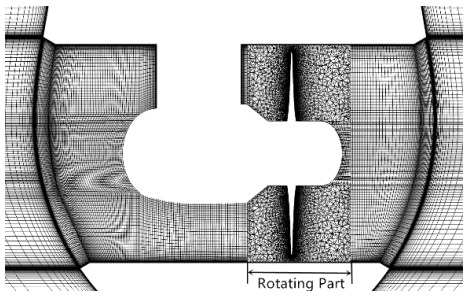

Figure 19: Grids inside the tunnel

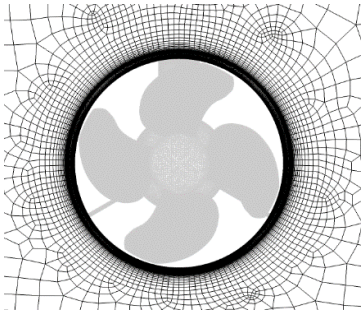

Figure 20: Surface grids around the entrance of the tunnel

The rest of the computational domain is defined in the fixed coordinate system, and is further divided into 80 sub-domains which are discretized with hexahedral cells. The cells near the tunnel wall, especially around the entrance and exit of the tunnel are densified and stretched to

resolve the large gradients of flow quantities, as shown in 20.

The grids are generated by using GAMBIT, a pre-processor of the software FLUENT. There are about 10 million cells for the entire domain, where 6 million are dedicated to the rotating part.

The flow around tunnel thrusters is simulated by solving the RANS equations, using the shear-stress transport (SST) *k-ω* model and Schneer & Sauer cavitation model for turbulence closure and cavitation simulation respectively. And for all the governing equations, the second-order upwind scheme is employed to discretize the convection terms.

The quasi-steady model is employed at first to improve the convergency of cavitation flow, then the unsteady sliding mesh model is applied to simulate the interactions between the rotating and stationary parts of the computational domain. The time step size is set as 2.469×10^{-4}s, which corresponds to an angular displacement of 2° for the impeller rotating speed of 22.5r/s. The environment pressure is set as 4.3×10^{3} Pa to meet with the requirement of σ_n=2.5.

The surfaces of impeller blades, the hub, the gearbox, the tunnel, and the hull are set as stationary walls in their respective coordinate systems. The outlet is set as a pressure outlet, and the inlet and other side faces as designated in Figure 18 (right) are set as velocity inlets. Only the bollard condition is simulated here, so the inlet velocity is set to zero. Since the experiment is conducted in the cavitation tunnel, a symmetry boundary condition is employed for the top of the computational domain instead of the free surface.

3.2 Numerical results and analysis

- **Cavity patterns**

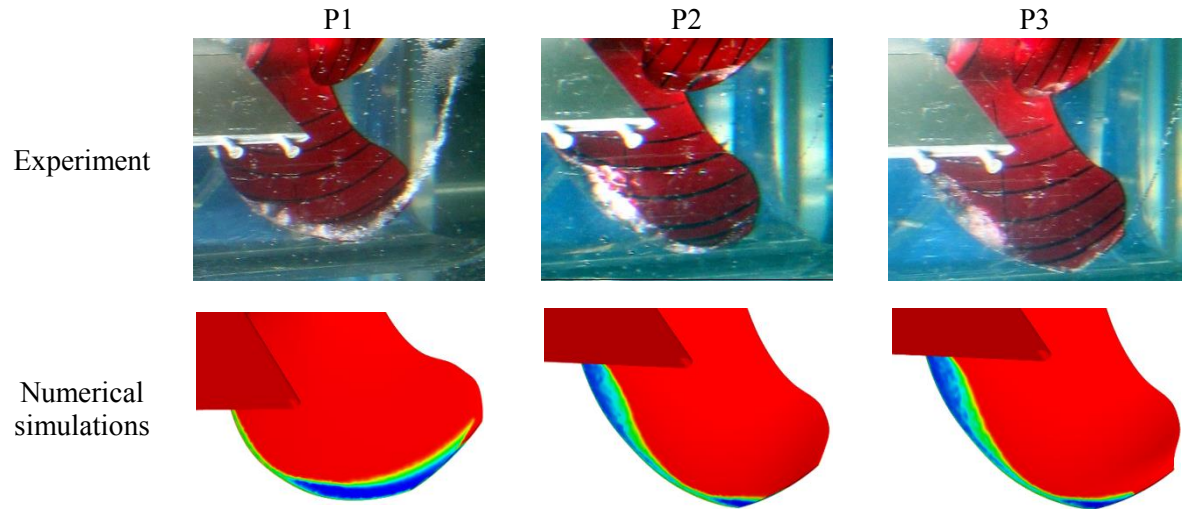

Figure 21: Comparison of cavity patterns for the three impeller models

As shown in Figure 21, the simulated cavitation patterns at σ_n=2.5 are quite similar to those observed in the experiments. The cavitation is reduced near the blade tip for impeller models P2 and P3 as a result of the tip-unloaded pitch distribution.

- **Fluctuating pressures**

The Fourier analysis results of the CFD simulated fluctuating pressures are compared with experimental results in Figure 22 ~ Figure 24. Figure 22 and Figure 24 indicate that the fluctuating pressure amplitudes at transducer S1 and S6 are well simulated.

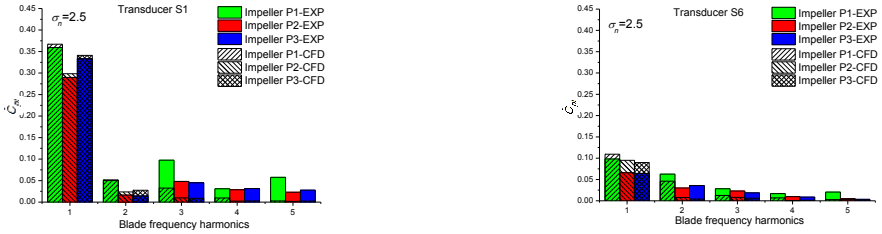

Figure 22: Comparison of fluctuating pressure amplitudes at transducer S1 and S6, $\sigma_n = 2.5$.

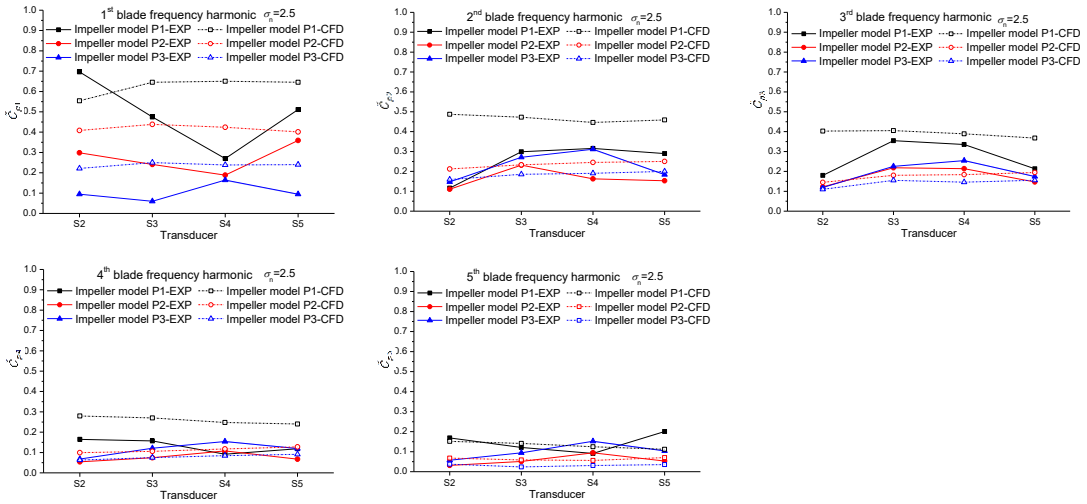

Figure 23: Comparison of fluctuating pressure amplitudesat transducers S2 through S5, σ_n=2.5.

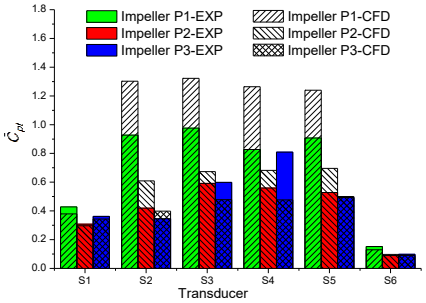

Figure 24: Comparison of the total amplitudes of fluctuating pressures at σ_n=2.5.

In Figure 23, the simulated fluctuating pressures exhibit a smoother distribution from transducer S2 to S5 than the experimental results. At all the five blade frequency harmonics and

on most transducers of impeller model P1 and P2, and at the 1st blade frequency harmonics of impeller model P3, the fluctuating pressures are over predicted by numerical simulation; while at 2nd~5th blade frequency harmonics of impeller model P3, the fluctuating pressures are under predicted. So the total fluctuating pressure amplitudes at transducers S2~S5 are over predicted for impeller model P1 and P2 and under predicted for impeller model P3 by the CFD simulations, as shown in Figure 24.

The present numerical results also indicate that unloading towards the tip (P2 and P3) can effectively reduce the cavitation induced fluctuating pressures, which is the same as what was found in the experiments. Furthermore, the numerical simulations suggest that a tip rake towards upstream can reduce the fluctuating pressures on the tunnel wall.

4 CONCLUSIONS

Model tests have been carried out for the tunnel thruster in the cavitation tunnel of Shanghai Jiao Tong University to investigate the effects of the pitch and rake distributions of impeller blades on fluctuating pressures on the tunnel wall. Viscous flow CFD simulations are also performed at one cavitating condition. A number of conclusions are drawn according to the experimental and numerical results,

(1) In both non-cavitating and cavitating conditions, the fluctuating pressures are higher at the impeller disk than at upstream in general, but attenuate quickly as it goes downstream. The fluctuating pressures induced by impeller P1 are significantly higher than those by P2 and P3, indicating that the 'flat plate' blade is unfavorable for vibration excitation, and unloading towards the tip as often adopted in open propeller design should be introduced in the impeller design.

(2) CFD simulation is a useful tool for predicting the impeller vibration performance under cavitating condition and the cavity patterns are well predicted. However, the accuracy of predicted fluctuating pressures is yet to be improved.

(3) It is not yet clear to the authors how the rake distribution near the tip influences the tip clearance flow in the case of a tunnel thruster. The fluctuating pressures of impeller P2 are both lower than those of P3 based on the experiments, which is different from the results of our RANS simulations. Further study is needed in this respect.

REFERENCES

[1] PEREIRA F, SALVATORE F, DI FELICE F, et al. Experimental and numerical investigation of the cavitation pattern on a marine propeller[C]//Proc. of the 24th Symposium on Naval Hydrodynamics. Fukuoka, Japan, 2002: 236-251.

[2] PEREIRA F, SALVATORE F, DI FELICE F, et al. Experimental investigation of a cavitating propeller in non-uniform inflow[C]//Proc. of the 25th Symposium on Naval Hydrodynamics. St.John's, Canada, 2004: 813-829.

[3] SALVATORE F, STRECKWALL H, TERWISGA T V. Propeller cavitation modelling by CFD - results from the VIRTUE 2008 Rome workshop[C]// Proc. of the 1st International Symposium on Marine Propulsors. Trondheim, Norway, 2009: 362-371.

[4] TANIGUCHI K, WATANABE K, KASAI H, et al. Investigation into the fundamental characteristics and operating performances of side thruster [R]. SR59, Tokyo, Japan: Japan Ship Technology Research Association (in Japanese), 1964.

[5] PEHRSSON L, MENDE R G. Design, model testing and application of controllable pitch bow thrusters [J]. Journal of the American Society for Naval Engineers, 1961, 73(4): 787-796.

[6] ENGLISH J W. Further considerations in the design of lateral thrust units [R]. NPL Report No.63, London, United Kingdom: National Physical Laboratory, 1964.

[7] BEVERIDGE J L. Design and performance of bow thrusters [R]. Report No.3611, America: Naval Ship Research and Development Center, 1971.

[8] MULLER S B, ABDEL-MAKSOUD M. Numerical investigationof transverse thrusters [R]. Humburg, Germany:University of Duisburg-Essen, 2007.

[9] YAO Z Q, YAN Z G. Hydrodynamic performance analysis and verification of transverse thrusters [J]. Journal of Ship Mechanics, 2012, 16(3): 236-245.

[10] YU C, YANG C J. Study of tunnel thruster performance and flow by quasi-steady Reynolds-Averaged Navier-Stokes simulation [J]. Journal of Shanghai Jiaotong University (Science), 2016, 21(6): 662-671.

[11] STEFANO G, LUCA S, STEFANO B, et al. Comparison of experimental measurements and numerical calculations for a propeller in axial cylinder [C]//Proc. of the 1st International Symposium on Marine Propulsors. Trondheim, Norway, 2009: 525-536.

[12] FISCHER R. Bow thruster induced noise and vibration[C]//Dynamic Positioning Conference 2000.Houston, USA: 2000.